Quantum control in quantum wells

Jeffrey L. Krause
Quantum Theory Project, P.O. Box 118435, University of Florida, Gainesville, Florida 32611

David H. Reitze and Gary D. Sanders
Department of Physics, P.O. Box 118440, University of Florida, Gainesville, Florida 32611

Alex V. Kuznetsov
Department of Physics, Ohio State University, Columbus, Ohio 43210

Christopher J. Stanton
Department of Physics, P.O. Box 118440, University of Florida, Gainesville, Florida 32611

(Received 2 July 1997)

We present calculations of quantum control of wave packet motion and THz emission in an asymmetric double-quantum-well structure. A genetic algorithm is used to search for the laser pulse that best drives an electronic wave packet to a desired target, or goal. The targets considered in this work include maximizing the overlap of an electronic wave packet with a given distribution at a specific time, and maximizing the induced THz emission from the quantum well. We also show that, assuming a fixed laser pulse, the parameters of the quantum well can be optimized to produce a desired outcome. Our results indicate that simple laser pulses are sufficient to exert control over the dynamics of charged carriers in engineered semiconductor heterostructures. [S0163-1829(98)06515-1]

I. INTRODUCTION

Recent advances in both the generation of ultrafast laser pulses and growth techniques for semiconductor heterostructures have led to extensive investigations of the coherent dynamics of charged carriers in semiconductors. High-quality semiconductor quantum wells and superlattices can exhibit transverse $(T2)$ dephasing times from tens of femtoseconds (for free carriers) to in excess of a few picoseconds (for excitonic coherences). These dephasing times, in favorable cases, are many times longer than the 10-fs time resolution available with current laser sources. This enables short-pulse lasers to be used as sensitive probes of the coherent interaction of electric fields with the induced polarization in heterostructure devices. The ability to create and detect wave packets constructed from charged carriers has led to the observation of many coherent phenomena, including Bloch oscillations in superlattices,[1,2] heavy and light hole quantum beats in quantum wells,[3] Rabi flopping in semiconductors,[4] coherent dynamics of excitonic wave packets,[5] wave-packet oscillations,[6] THz emission from asymmetric double quantum wells (ADQW),[7] and, most recently, far-infrared emission from asymmetric quantum wells.[8]

While ultrafast optical excitation provides a method for observing coherent dynamics in semiconductor heterostructures, it also offers intriguing possibilities for controlling the dynamics of coherent interactions and manipulating electronic wave packets. A number of experimental papers have recently explored these concepts. For example, experiments by Planken *et al.*[9,10] have demonstrated an enhancement in terahertz radiation generated from biased ADQWs using pairs of phase-locked femtosecond pulses to coherently excite and amplify quantum beating. Dupont *et al.*[11] have shown that the direction of photocurrent in n-doped quantum wells can be controlled by irradiating the sample simultaneously with the fundamental of a laser beam and its second harmonic. By adjusting the phase difference between the two beams, asymmetric interference is created in the continuum electronic wave functions. Similar results using two-pathway control of photocurrents have been demonstrated recently in bulk GaAs by Atanasov *et al.*[12] In another application, Heberle *et al.*,[13] using phase-locked pulses tuned to exciton resonances, have demonstrated population control and coherent destruction of heavy hole excitons in quantum wells. One common feature in all of these experiments is that the laser excitation conditions necessary to achieve control can be guessed intuitively, due to the relatively simple dynamics involved in the systems under study.

For the most general and complex quantum-mechanical systems and corresponding control goals (for example, shaping THz radiation or controlling charge motion in complex heterostructures), simple intuition fails to discern the best optical excitation scheme and more sophisticated methods must be employed. For example, complex filters can be designed to synthesize phase-tailored pulses that enhance THz radiation in biased ADQWs.[14,15] More generally, detailed proposals using some variant of optical control theory to guide the evolution of quantum-mechanical systems with lasers date back at least twenty years.[16] The concept has received considerable attention recently, particularly in the development and application of theoretical methods.[17–21] In addition, substantial experimental progress has been made in the synthesis of temporally tailored ultrafast wave forms.[22–25] Femtosecond pulse shapers employ programmable phase and amplitude modulators in the Fourier plane

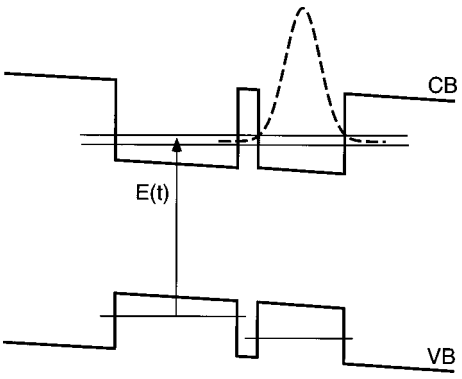

FIG. 1. Schematic of the dc-biased asymmetric double quantum well discussed in this work. The excitation is to the wide well, and the target (shown as a dashed line) consists of a transform-limited Gaussian wave packet centered in the narrow well.

of a grating/lens apparatus to apply a complex frequency-dependent phase and amplitude profile to the input pulse spectrum. The resulting output temporal wave forms are then the inverse Fourier transform of the filtered pulse spectrum. Pulse shaping methods have been used to synthesize complex pulses with both high frequency,[22,23] and temporal resolution.[25] These pulses have been used in experiments to mode-selectively excite coherent phonons in molecular crystals.[26] Nevertheless, almost no effort to date has been directed at applying these ideas to engineered semiconductor heterostructures.

In this paper, we examine the possibility that shaped, ultrafast laser pulses can be used to control the carrier dynamics and THz emission in quantum wells. Our investigations explore the dynamics of semiconductor heterostructures in the regime in which the optical fields interact with the evolving states at or near the time scale of the dynamics. In particular, the laser excitation is not assumed to be impulsive. There are several motivations for our studies. First, quantum wells and superlattices are textbook quantum-mechanical systems that should provide model environments for examining the feasibility of control methods for influencing the coherent dynamics of electrons and holes. In addition, solid state heterostructures provide a stringent test for judging the effectiveness of optimal control methods in quantum systems that exhibit fast dephasing times. Finally, controlling the ultrafast motion and interactions of charged carriers in semiconductors is potentially important from a technological standpoint and may lay the groundwork for a new class of solid state optoelectronic devices that operate on picosecond time scales.

We consider in this work a simple and widely studied quantum-mechanical system, an asymmetric double quantum well (see Fig. 1). Application of a dc bias field causes the electronic levels in the conduction band to move into tunneling resonance, while the hole levels in the valence band move out of tunneling resonance. When the ADQW is excited by a sufficiently broadband, ultrafast laser pulse tuned to an exciton resonance in one of the wells, an electronic wave packet (a coherent superposition of two or more states) is created in the conduction band that oscillates back and forth from the narrow well to the wide well. The ADQW system has been used previously to demonstrate coherent wave packet oscillation,[6] coherent THz emission,[7] and two-pulse control of wave-packet dynamics.[27] From the viewpoint of control, the ADQW offers two enticing possibilities, control of the evolution of the electronic wave packet, and control of the induced THz emission resulting from the acceleration of the charged carriers as they oscillate in the wells.

The paper is organized as follows. In Sec. II, we outline the theoretical treatment, and describe the methods used to predict the optimal laser fields. Results for control of wave-packet motion are presented in Sec. III. We show that optimizing either the laser field or the spatial confinement potential results in enhancement and control of wave-packet motion. We also demonstrate that coherent THz radiation can be enhanced using optimized laser pulses, and show that, for a fixed laser pulse, the parameters of the ADQW can be optimized to produce a desired result. A general discussion of our results is presented in Sec. IV, where we examine some specific issues associated with applying the methods of quantum control to electronic states in heterostructures. In particular, we discuss the effects of dephasing, Coulomb effects, light hole excitons, and the role of extended electronic k states in the computation of optimal laser fields. Finally, in Sec. V, we discuss the prospects for experimental verification of our predictions, and conclude.

II. GENERAL THEORY

A. Electronic states in the ADQW

The general theory is an extension of that developed by Kuznetsov *et al.*,[28] modified to treat the system described here, the asymmetric double quantum well. We begin by deriving the k-dependent solutions of a biased ADQW driven by a complex laser field. The complete wave functions, $\varphi^{\alpha}_{n,\mathbf{k}}(\mathbf{r})$, for confined carriers in the ADQW depicted in Fig. 1 are obtained by multiplying the band edge bulk Bloch states, $u^{\alpha}(\mathbf{r})$, by a slowly varying envelope function. Thus,

$$\varphi^{\alpha}_{n,\mathbf{k}}(\mathbf{r}) = \frac{e^{i\mathbf{k}\cdot\mathbf{r}}}{\sqrt{A}} F^{\alpha}_{n}(z) u^{\alpha}(\mathbf{r}), \tag{1}$$

where $\alpha = c,h,l$ labels the carrier type (electron, heavy-hole, or light-hole, respectively) as well as the spin index, and n labels the subband index. The *complete* envelope function consists of a plane wave (with cross-sectional area A and wave vector $\mathbf{k}$) describing translational motion in the x-y plane multiplied by a slowly varying function $F^{\alpha}_{n}(z)$ that describes the confined motion of the carriers along the z axis.

Within the quantum well, the envelope functions $F^{\alpha}_{n}(z)$ satisfy a one-dimensional, effective-mass Schrödinger equation,

$$\left[-\frac{\hbar^2}{2m_{\alpha\perp}} \frac{d^2}{dz^2} + V_{\alpha}(z) \pm e\mathcal{D}z \right] F^{\alpha}_{n}(z) = E^{\alpha}_{n} F^{\alpha}_{n}(z), \tag{2}$$

where $m_{\alpha\perp}$ is the effective mass along the z direction and $\mathcal{D}$ is the dc field. In the third term, the upper sign $(+)$ is used for holes, and the lower sign $(-)$ is used for electrons. The potential $V_{\alpha}(z)$, which appears in the effective-mass equation, is the confining potential of the ADQW.

The ADQW band structure consists of a set of parabolic subbands. The electronic subband energies are given by

$$E_n^c(k) = E_g + E_n^c + \frac{\hbar^2 k^2}{2m_{c\|}} \tag{3}$$

and for heavy and light holes, the subband energies are

$$E_n^h(k) = -E_n^h - \frac{\hbar^2 k^2}{2m_{h\|}} \tag{4}$$

and

$$E_n^l(k) = -E_n^l - \frac{\hbar^2 k^2}{2m_{l\|}}, \tag{5}$$

respectively. The effective masses are determined from the Luttinger parameters,[28] and the subband energies E_n^α and envelope functions $F_n^\alpha(z)$ are determined by solving Eq. (2) numerically on a finite difference grid. The numerical procedures have been described in detail previously.[28]

B. Density matrix for the ADQW

We define the density matrix in terms of the ADQW eigenstates. Let $a_{n,\mathbf{k}}^{\alpha\dagger}(t)$ and $a_{n,\mathbf{k}}^{\alpha}(t)$ be the Heisenberg operators that create and destroy electrons in a state $\varphi_{n,\mathbf{k}}^{\alpha}(\mathbf{r})$. The density matrix (DM) is

$$N_{nm,\mathbf{k}}^{\alpha\beta}(t) \equiv \langle a_{n,\mathbf{k}}^{\alpha\dagger}(t) a_{m,\mathbf{k}}^{\beta}(t) \rangle, \tag{6}$$

where $\langle\ \rangle$ denotes the statistical average of the current nonequilibrium state of the system, and α,β represent the conduction band electrons and the valence band heavy and light holes.

The interband components of the density matrix, $N_{nm,\mathbf{k}}^{\alpha\beta}(t)$, $\alpha \neq \beta$, describe the coherence between different carriers, α and β, in subbands n and m, respectively, and are related to the optical polarization. The intraband components of the density matrix, $N_{nm,\mathbf{k}}^{\alpha\alpha}(t)$, describe correlations between different subbands of the same carrier type if $n \neq m$. If $n = m$, $N_{nn,\mathbf{k}}^{\alpha\alpha}(t)$ is just the number of carriers in the quantum-well state $\varphi_{n,\mathbf{k}}^{\alpha}(\mathbf{r})$.

C. Bloch equations

The density matrix obeys the general equation of motion

$$-i\hbar \frac{\partial N_{nm,\mathbf{k}}^{\alpha\beta}(t)}{\partial t} = \langle [H_{\mathbf{k}}, N_{nm,\mathbf{k}}^{\alpha\beta}(t)] \rangle, \tag{7}$$

where the square brackets denote the commutator. The Hamiltonian operator for a quantum well interacting with a plane-polarized radiation field incident along z and polarized along x is

$$H_{\mathbf{k}} = \sum_{\alpha n} \varepsilon_n^\alpha(k) a_{n\mathbf{k}}^{\alpha\dagger}(t) a_{n\mathbf{k}}^{\beta}(t) - E^{\mathrm{opt}}(t) \sum_{\alpha\beta,nm} d_{nm,\mathbf{k}}^{\alpha\beta} a_{n\mathbf{k}}^{\alpha\dagger}(t) a_{m\mathbf{k}}^{\beta}(t), \tag{8}$$

where $E^{\mathrm{opt}}(t)$ is the time-dependent optical electric field (with unit polarization vector assumed to be $\mathbf{x}$) and $d_{nm,\mathbf{k}}^{\alpha\beta}$, the projection of the electron dipole moment along $\mathbf{x}$ is

$$d_{nm,\mathbf{k}}^{\alpha\beta} = \int d\mathbf{r}\ \varphi_{n\mathbf{k}}^{\alpha}(\mathbf{r}) ex \varphi_{m\mathbf{k}}^{\beta}(\mathbf{r}). \tag{9}$$

The first term in Eq. (8) governs the creation and destruction of the states in the ADQW, as discussed above. The second term represents the interaction of these states with a coherent optical field $E^{\mathrm{opt}}(t)$. Previous work considered only a transform-limited, Gaussian temporal profile for the laser field.[28] Here we allow for a more general optical field to include such complicated effects such as high-order phase dispersion and non-Gaussian, frequency-dependent amplitudes. As indicated below, the parameters of the optical field can be varied to exert control over the charge carriers.

Since the ADQW is excited with optical pulses, we can neglect intraband transitions (i.e., dipole transitions for which $\alpha = \beta$). The dipole matrix elements for optical transitions can then be calculated using a procedure described previously.[28] If we substitute the Hamiltonian [Eq. (8)] into the equation of motion, we get the Bloch equations for the components of the density matrix

$$\frac{\partial N_{nm,\mathbf{k}}^{\alpha\beta}}{\partial t} = i\left(\frac{E_n^\alpha(k) - E_m^\beta(k)}{\hbar}\right) N_{nm,\mathbf{k}}^{\alpha\beta} + i \frac{E^{\mathrm{opt}}(t)}{\hbar} \sum_{\gamma j} (N_{nj,\mathbf{k}}^{\alpha\gamma} d_{jm}^{\gamma\beta} - d_{nj}^{\alpha\gamma} N_{jm,\mathbf{k}}^{\gamma\beta}). \tag{10}$$

Note that by retaining in the Hamiltonian only the interaction with the electric field [Eq. (8)], a different set of equations is obtained for each wave vector k, and the statistical averages that appear in the Bloch equations are independent elements of the density matrix. This is a considerable simplification, and makes the problem computationally tractable. Including the Coulomb interactions in the Hamiltonian requires a statistical average over products of two creation operators and two annihilation operators. While, in principle, one could decouple statistical averages over four operator products into products of density matrix elements, the resulting equations would be coupled for different values of k, and would require substantial computational resources to solve. To focus on the basic physical picture, and how it relates to control, we concentrate here on the less complex model in Eq. (10).

Equation (10) can be solved by using the rotating-wave approximation (RWA) and retaining only those terms in the Bloch equations that are close to resonance with the free oscillations of the density matrix. The resulting set of Bloch equations can then be solved using an adaptive step-size Runge-Kutta routine.[28]

D. Densities, dipole moments, and THz signals

At a fixed value of k, the particle density,

$$P_{\mathbf{k}}(\mathbf{r},t) = \langle \psi_{\mathbf{k}}^\dagger(\mathbf{r},t)\, \psi_{\mathbf{k}}(\mathbf{r},t) \rangle, \tag{11}$$

can be calculated from the envelope functions $F_n^\alpha(z)$ and density matrix as

$$P_{\mathbf{k}}(\mathbf{r},t)=\sum_{\alpha\beta,nm}\frac{F_n^{\alpha}(z)^*F_m^{\beta}(z)}{A}u^{\alpha}(\mathbf{r})^*u^{\beta}(\mathbf{r})N_{nm,\mathbf{k}}^{\alpha\beta}(t). \tag{12}$$

The sum over band indices contains two interband terms whose contribution to the overall charge density oscillates in time with the interband frequency. This contribution leads to the interband current that interacts with the optical field. However, for times longer than the inverse band gap (about 0.5 fs for GaAs), the interband terms will average to zero. Since we are interested in quantities that vary in time on the much longer time scale of the excitation envelope (typically 100 fs), we can safely omit the interband terms. This is equivalent to averaging the particle density over unit cells. The result is

$$P_{\mathbf{k}}(\mathbf{r},t)=\sum_{\alpha,nm}\frac{F_n^{\alpha}(z)^*F_m^{\alpha}(z)}{A}n_{nm,\mathbf{k}}^{\alpha}(t). \tag{13}$$

The total carrier density (electrons and holes) is obtained by summing the above expression over the wave vector **k**. We can write this as a sum over the total number density for each carrier type α, which is given by

$$\rho^{\alpha}(z,t)=\sum_{n,m}F_n^{\alpha}(z)^*F_m^{\alpha}(z)\frac{1}{2\pi}\int_0^{\infty}dk\ k\ \mathrm{Re}[N_{nm,k}^{\alpha\alpha}(t)]. \tag{14}$$

The dipole moment is written in terms of the charge density as

$$\mathbf{d}(t)=\sum_{\alpha}\int dz\ ez\rho^{\alpha}(z,t)\hat{z}, \tag{15}$$

and the THz signal is proportional to the second derivative of the time-dependent dipole moment.

E. Simplified theory

For a specific laser field $E^{\mathrm{opt}}(t)$, the solution for the time-dependent density matrix can be computed from Eq. (10). However, for optimization purposes, the above theory is somewhat cumbersome, because it requires a solution of a system of differential equations, one equation for each k state. In the presence of Coulomb interactions, the situation is even worse, because the equations are coupled. Our goal, in this work, is to determine the laser field that best drives the system to a desired outcome, or goal. This requires, in general, solving the equations of motion for many different fields. To proceed, we invoke a set of physically reasonable approximations that simplify the problem and greatly increase the computational efficiency, while still preserving the main physical features.

We begin by assuming that the excitation occurs at zone center from a single heavy-hole level in the valence band, and creates a superposition of two (or more) electronic levels in the conduction band. This assumption is valid in the case of the biased double quantum well, and might also be realized in strained layer systems, in which the quasidegeneracy of the heavy and light holes is lifted. The total Hamiltonian can then be written as

$$H(t)=H_0-DE^{\mathrm{opt}}(t), \tag{16}$$

where H_0 is the Hamiltonian for carrier motion given in Eq. (2), D is the dipole operator, and $E^{\mathrm{opt}}(t)$ is the laser field. Under the assumption that the dynamics involves only a heavy hole in the valence band, and electrons in the conduction band, the time-independent material Hamiltonian becomes

$$H_0=H^h|h\rangle\langle h|+[H^c+\omega_{hc}]|c\rangle\langle c|, \tag{17}$$

where H^h and H^c are the Hamiltonians for heavy holes and electrons, respectively, and ω_{hc} is the center frequency of the laser. The dipole operator D is then

$$D=\mu_{hc}\{|h\rangle\langle c|+|c\rangle\langle h|\}, \tag{18}$$

where μ_{hc} is the dipole moment connecting the hole states in the valence band with the electron states in the conduction band. The total envelope function $|F(t)\rangle$ in the confined dimension is a solution of the time-dependent Schrödinger equation,

$$i\frac{d}{dt}|F(t)\rangle=[H_0-DE^{\mathrm{opt}}(t)]|F(t)\rangle, \tag{19}$$

and consists of a sum of the hole envelope function and the electron envelope function,

$$|F(t)\rangle=|F^h(t)\rangle|h\rangle+|F^c(t)\rangle|c\rangle. \tag{20}$$

Since, in this approximation, the envelope functions for both the hole and the electron are pure states, they can be expanded in eigenstates of the time-independent hole and electron Hamiltonians, $|\phi_n^h\rangle$ and $|\phi_n^c\rangle$, respectively,

$$|F^h(t)\rangle=\sum_n a_n^h(t)|\phi_n^h\rangle, \tag{21}$$

and

$$|F^c(t)\rangle=\sum_n a_n^c(t)|\phi_n^c\rangle. \tag{22}$$

Then, in first-order perturbation theory, we assume that the initial hole level is an eigenstate $|\phi_i^h\rangle$ (or, more appropriately, that the laser field is only on resonance with one hole state), and that $a_i^h=\delta_{ni}$ and $\dot{a}_n^h=0$. That is, the laser field is weak in the sense that the amount of population excited in the conduction band is small, and scales linearly with the laser intensity. This is strictly true only at the very beginning of the Rabi cycle, but experience shows that the approximation is reasonable even for significant population transfers (up to $\sim$25%).[29] Finally, the envelope function in the conduction band can be written in the rotating-wave approximation as

$$|F^c(t)\rangle=\sum_n|\phi_n^c\rangle e^{-i\omega_{nc}t}\langle\phi_n^c|\mu_{hc}|\phi_i^h\rangle\times\int_{-\infty}^{t}d\tau\ E^{\mathrm{opt}}(\tau)e^{-i(\omega_{nc}-\omega_{hi})\tau}. \tag{23}$$

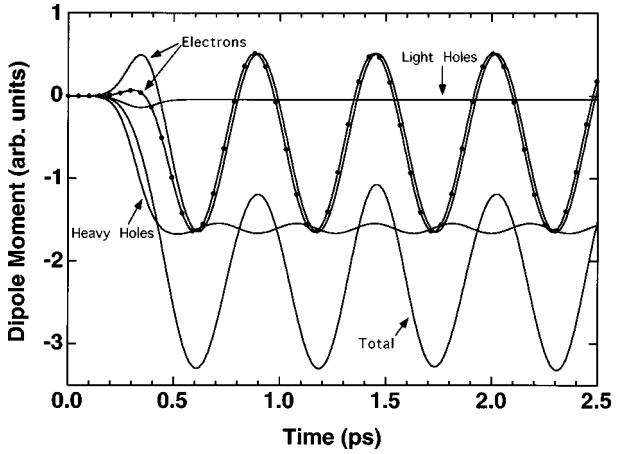

FIG. 2. Comparison of the time-dependent dipole moments calculated with the full theory and the simplified theory, as described in the text. The total dipole moment for the more elaborate theory contains contributions from the electrons, light holes, and heavy holes. The dipole moment for the simplified theory (filled circles) contains only contributions from the electrons. Results from the two methods have been scaled to the same electronic population.

This expression, once the electron and hole eigenstates have been calculated, can be evaluated efficiently for any laser field. This is crucial for the optimization procedure, as discussed below.

To verify the validity of these approximations, we compare the time-dependent dipole moments computed by the theory as presented in Sec. II with the simplified version described in this section. The full theory includes the proper number (as determined by the bandwidth of the excitation pulse) of heavy holes, light holes, and electronic k states. It does not include Coulomb interactions. The results of a typical test calculation are shown in Fig. 2, which compares the time-dependent dipole calculated with the simplified theory, and the more elaborate theory. In the simple theory, the only contribution to the dipole is from the electrons. The more elaborate theory contains contributions from the electrons, heavy holes, and light holes. In the case considered, two heavy-hole levels and one light-hole level are contained within the frequency bandwidth of the excitation pulse. Comparing the electronic dipoles in the two methods shows that the integration over k affects mainly the initial rise of the dipole. In general, the results of the two theories are qualitatively similar, indicating that the simplified theory provides a reasonable starting point for optimization of the laser pulse, and interpretation of experiments. In particular, we note that the dominant contribution to the total time-dependent dipole is from the electrons.

F. Optimal control theory

Equation (23), or equivalently Eq. (14), in the more complete version of the theory, allows us to calculate the wave function or density matrix produced by a specific laser field. Here, we propose to ask the inverse question. That is, given a specific target or objective that we wish the wave function to achieve, what is the laser field that best drives the system to that objective? To answer this question, we begin by constructing a target operator $\hat{A}$, which specifies the desired outcome. In general, $\hat{A}$ is a projection operator onto a set of observables specified by the target. The objective is to maximize the target yield, or the expectation value of $\hat{A}$ at a chosen target time t_f,

$$A(t_f)=\langle\psi(t_f)|\hat{A}|\psi(t_f)\rangle \tag{24}$$

or

$$A(t_f)=\mathrm{Tr}\hat{A}\rho(t_f). \tag{25}$$

To prevent the optimization procedure from discovering trivial, or nonphysical solutions, the yield A must in general be optimized with respect to a set of constraints. These constraints can take many forms, including, for example, details of the experimental apparatus and the system being measured.

In this work, we choose to impose a constraint on the total intensity, or fluence, of the laser field, which prevents the procedure from discovering solutions with zero or infinite field strength. To do this we write a control functional J,[30–37]

$$J=A-\lambda\int dtE(t)^2, \tag{26}$$

containing the yield and the constraint. In this particular case, the Lagrange multiplier λ has a specific interpretation, namely, the optimal yield with respect to the incident energy of the laser field.[36] Notice that J depends on the laser field $E(t)$ both explicitly via the constraint, and implicitly, via the yield. To find the optimal fields, we perform a functional variation of J, and set the first-order variation equal to zero. The resulting equations must in general be solved iteratively for the optimal fields.[30–37]

As a first example, consider the case in which the target is an electronic state in the conduction band

$$\hat{A}=\hat{A}_c|c\rangle\langle c|. \tag{27}$$

For further simplicity, we assume that $\hat{A}_c$ is a projection operator onto a pure state $|\Phi_c\rangle$, or

$$\hat{A}_c=|\Phi_c\rangle\langle\Phi_c|. \tag{28}$$

Then, in the perturbative regime as discussed above, the yield can be expanded in a power series about the optimal field. The lowest-order, nontrivial contribution to the yield is the second-order term,[36,37]

$$A_c^{(2)}(t_f)=\int_{-\infty}^{t_f}d\tau\int_{-\infty}d\tau' M_c^S(\tau,\tau')E^*(\tau)E(\tau'). \tag{29}$$

The symmetrized control kernel $M_c^S(\tau,\tau')$,

$$M_c^S(\tau,\tau')=[M_c^S(\tau',\tau)]^*=M_c(t_f-\tau,\tau-\tau'), \tag{30}$$

for the target in Eq. (28) can be written as

$$M_c(t_2,t_1)=\langle\psi_c^0(t_2)|\Phi_c\rangle\langle\Phi_c|\psi_c^0(t_1+t_2)\rangle, \tag{31}$$

where

$$|gw_c^0(t)\rangle=\sum_n|\phi_{nc}\rangle e^{-iE_{ni}t}\langle\phi_{nc}|\mu_{hc}|\phi_{hi}\rangle. \tag{32}$$

The optimal fields are then computed as solutions of an eigenequation by discretizing the control kernel onto a numerical grid, over a specified time interval,[36,37]

$$\int_{t_0}^{t_f} d\tau' M_c^S(\tau,\tau')E(\tau') = \lambda E(\tau). \tag{33}$$

The eigenvalues λ are the target yields, and the eigenvectors are the optimal fields $E(t)$. The eigenvector associated with the largest eigenvalue is the globally optimal field, in the perturbative limit.

To determine how well a given field performs, we define an achievement $\alpha(t)$,[37]

$$\alpha^2(t) = \frac{|\langle \Phi_c|\psi_c(t)\rangle|^2}{\langle \Phi_c|\Phi_c\rangle\langle \psi_c(t)|\psi_c(t)\rangle}, \tag{34}$$

which in this case is simply the normalized overlap of the wave function with the target. The achievement is constructed to range from zero (no control) to one (perfect control).

In some cases, the above procedure for determining the optimal fields is inconvenient, either for computational reasons, or because the control functional does not take the simple quadratic form of Eq. (26). For these situations, an alternative procedure can be applied. We assume that the laser field $E(t)$ can be adequately described by a small number of parameters, and then vary the parameters to optimize the yield. For example, assume that the laser field can be written as

$$E(t) = E_0 e^{-(t-\bar{t})^2/\Gamma^2} e^{-i\phi(t)}, \tag{35}$$

where E_0 is the amplitude, $\bar{t}$ is the center time, and $\Gamma\sqrt{\ln 16}$ is the temporal width (full width at half maximum). As conventionally, $\phi(t)$, the time-dependent phase, can be expanded in a Taylor series,

$$\phi(t) = \phi + \omega(t-\bar{t}) + \tfrac{1}{2}b(t-\bar{t})^2 + \cdots, \tag{36}$$

where ϕ is the (irrelevant) phase constant, ω is the center frequency, and b is the linear chirp. In the perturbative limit, the amplitude E_0 is also irrelevant, since the yield simply scales linearly with the amplitude of the field. The four remaining parameters, $\bar{t}$, Γ, ω, and b, are sufficient to characterize the laser field for a large variety of experimental conditions.

We have found that traditional methods for searching for the optimal parameters, such as conjugate gradient and simplex, are not adequate to determine the optimal laser parameters, because these methods tend to get trapped in local minima. In this work, we adopt a genetic algorithm (GA), which rapidly discovers the optimal fields.[38,39] The GA is a general purpose functional minimization routine, and requires as input an evaluation, or test function. In this case, the test function is simply the achievement [Eq. (34)]. Typically several thousand evaluations of the test function are required to maximize the achievement. This, however, is no difficulty in the simple, pure-state model discussed above, and is the main reason for presenting and implementing the simplified theory.

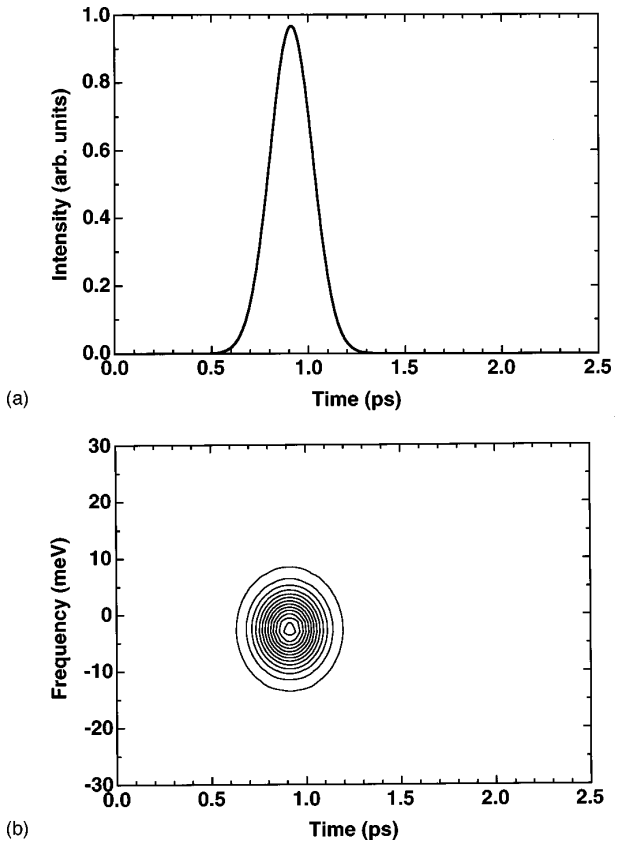

FIG. 3. Globally optimal field for the control scenario in Fig. 1. Panel (a) shows the intensity profile $|E(t)|^2$, and panel (b) shows the time-frequency (Wigner) distribution.

III. RESULTS

Figure 1 shows a schematic of the ADQW discussed above. As a first example of control in quantum wells, we choose a target consisting of a Gaussian distribution located in the narrow well. The object is to find the laser field $E(t)$ that creates a wave packet, initially in the narrow well, that evolves to maximum overlap with the target at the target time t_f. The field is constrained to the form in Eq. (36); and we use the genetic algorithm to optimize the parameters ω, t, Γ, and b.

The intensity envelope $|E(t)|^2$ of the optimal field discovered by the GA for the target in Fig. 1 is shown in Fig. 3(a). A time/frequency (Wigner) distribution $F_W(t,\omega)$ of this field is shown in Fig. 3(b). The Wigner distribution is defined as

$$F_W(t,\omega) = 2\,\mathrm{Re}\int_0^\infty d\tau e^{-i\omega\tau} E^*(t+\tau/2)E(t-\tau/2)W(\tau), \tag{37}$$

where $W(\tau)$ is a Gaussian window function included to remove self-interference. The advantage of this definition of the Wigner function is that integration over frequency gives the field strength $|E(t)|^2$, and integration over time gives the power spectrum, $|E(\omega)|^2$. We note that the locally optimal field in Fig. 3 is nearly identical to the globally optimal field calculated with Eqs. (28)–(33). The optimal field contains

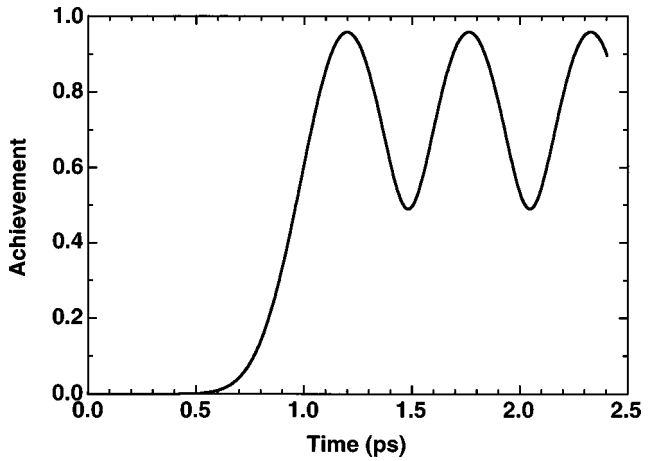

FIG. 4. Achievement (normalized overlap of the time-dependent wave packet with the target) of the optimal field in Fig. 2, for the scenario in Fig. 1.

very little chirp (that is, the parameter b is very close to zero), and so control for this target is simply a timing problem, provided that the laser pulse has the appropriate center frequency.

Figure 4 shows the achievement [Eq. (34)] as a function of time for the target shown in Fig. 1, with the optimal field depicted in Fig. 3. We can see that the target time in this case (or, more precisely, the time duration over which the control field is allowed to act) is long enough that three oscillations of the wave packet through the wide well can occur. The achievement reaches its maximum value of 0.97 at the target time, indicating nearly perfect control. The achievement in Fig. 4 is closely related to the expected signal observed in, for example, a transient absorption or emission experiment. Note, though, that this model assumes no dephasing. In reality, coherent oscillations would be damped in time by phase-breaking scattering events. We return to this issue below.

With the observation that the parameters most important to control in this example are the frequency, delay time, and the pulse width, we can construct control maps plotting the achievement of one parameter versus another. Two such maps are shown in Fig. 5. Figure 5(a) shows the delay time versus the frequency, and Fig. 5(b) shows the pulse width versus the frequency. In both figures, the achievement shows regions of nearly perfect control and regions of almost no control. The most sensitive parameter is the frequency, while the other parameters show broad plateaus of nearly constant achievement. Such maps indicate that the experimentalist, simply by varying an experimentally accessible parameter, can exert a large degree of control on the dynamics of the electronic wave packet. This observation forms the basis for the design of an experiment, as discussed below.

Wave packet control is only one possible type of control in the ADQW. Another possibility is to control the THz emission. To calculate the THz signal, we first compute the time-dependent dipole,

$$d(t) \propto \langle \psi(t) | z | \psi(t) \rangle. \tag{38}$$

The THz signal $s(t)$ is proportional to the second derivative of the dipole,

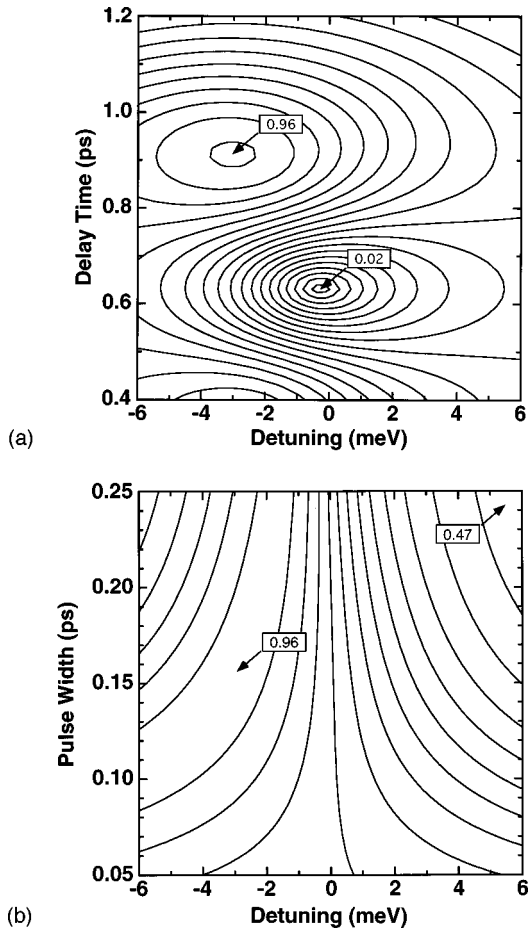

FIG. 5. Achievement as a function of various laser parameters in Eqs. (35) and (36). Panel (a) shows the variation with respect to the delay time between the pump pulse and the probe pulse, and the detuning of the center frequency of the probe pulse from the miniband center in the conduction band, and panel (b) is for the temporal pulse width versus the detuning.

$$s(t) \propto \frac{\partial^2}{\partial t^2} d(t). \tag{39}$$

As one example of a possible control scenario, we choose to maximize the THz signal at a particular time. In this case, the procedure discussed above to determine the globally optimal field is much more complicated, because the control functional is not quadratic. To overcome this difficulty, we use the genetic algorithm to discover the optimal pulse parameters. The results are shown in Fig. 6.

Figure 6(a) shows the intensity envelopes of two optimal fields. In both cases, the parameters are allowed to vary freely. However, in the first field (labeled A), the center time is not allowed to exceed 0.5 ps, and so the laser pulse cannot overlap the target time. In the second field (labeled B), no restriction is placed on the delay time. The fields in Fig. 6(a) look fairly similar, but in fact they are not. The Wigner distribution of these fields is shown in Fig. 6(b), where it can be seen that the first field is nearly transform-limited, with a slight negative chirp, while the second has a significant positive chirp (visible as the overall slope of the contours). The THz signal resulting from these two fields is shown in Fig. 7. Both signals exhibit a maximum at the target time. In the

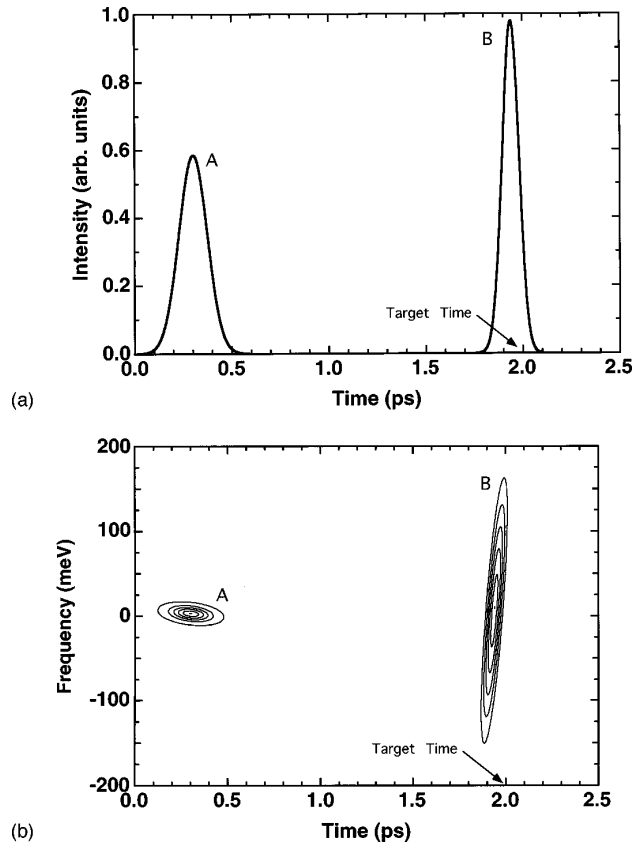

FIG. 6. Globally optimal fields for a target which specifies that the THz emission should reach a maximum at a target time of 2.0 ps. For pulse A, the parameters in Eqs. (35) and (36) are allowed to vary freely, except that the center time is restricted to be less than 0.5 ps. For pulse B, all parameters are allowed to vary freely. Panel (a) shows the intensity profiles $|E(t)|^2$, for the two pulses, and panel (b) shows the time-frequency (Wigner) distributions.

first case, the system times the oscillations so that a maximum is achieved at the target time. In the second case, however, the system discovers that using a chirped pulse that partially overlaps the target time creates an intense peak in the THz signal at the target time.

As a final example of control, we consider the case in which the laser pulse is assumed to be fixed, and the parameters of the well are optimized. In particular, we allow the widths of the wide well, the narrow well, and the barrier to vary, along with the magnitude of the dc field (and hence the splitting of the energy levels). While these parameters cannot be varied in real time in an experiment (except, perhaps, for the dc field), once designed, the optimal well can be grown easily. Figure 8(a) shows the results of a calculation in which we choose a target located, as previously, in the wide well. We (arbitrarily) restrict the parameters of the laser field so that the achievement is relatively low. The solid line shows the wave packet at the target time produced by this field. In this case the maximum achievement is only about 0.72. Allowing the parameters of the well to vary, however, produces the final wave packet shown in Fig. 8(b), with an achievement of 0.97. The optimized quantum well, and the original well, are compared in Fig. 9. As can be seen in the figure, fairly small variations in the parameters of the well (a change of $+6$ Å in the width of the wide well, and -17 Å in the narrow well) and the dc field bias ($+3.6$ kV/cm) are sufficient to dramatically enhance the achievement. In this case, the change in the dc field (about 34%) appears to have the most important effect.

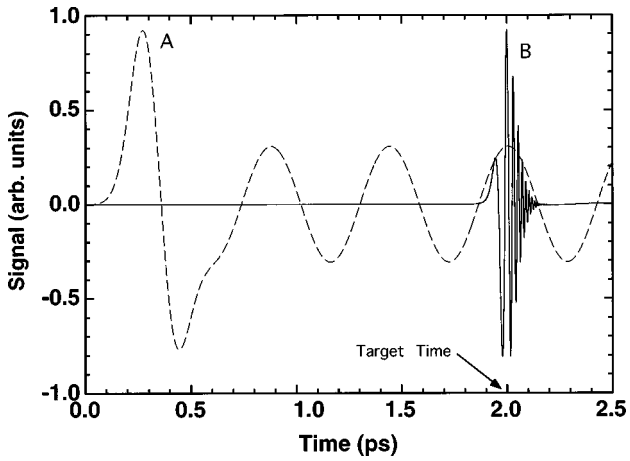

FIG. 7. THz signals for the two pulses shown in Fig. 6. Note that both pulses achieve a maximum at the target time.

IV. DISCUSSION

The results in the previous section indicate that significant control of carriers and THz emission is possible using appropriately tailored laser fields. The ADQW was chosen as a model heterostructure for its simplicity and for comparison with experimental data. However, several simplifications and approximations have been made in this work that, while enabling us to employ efficient optimization algorithms, neglect some of the fundamental interactions of electron-hole dynamics in semiconductor, quantum-confined structures. We now examine to what extent these approximations are valid and how they might compromise our ability to control wave-packet dynamics in heterostructures.

Using a simplified perturbative theory, we have treated the biased ADQW as a one-dimensional system in a single-particle picture in which photogenerated electron and hole states act independently. We have not included scattering mechanisms, which result in phase breaking and loss of wave-function coherence. Dephasing will ultimately place an upper limit on the time scale over which control can be exerted. Coulombic effects (excitons) have also not been included, nor have we yet considered how the dynamics of the heavy holes and light holes affect the control. In the experiments done to date on ADQWs, excitonic wave packets have been used because of their comparatively long dephasing times. Our simplified, one-dimensional calculations inherently neglect nonzero k states, and the free-particle nature of the energy band dispersion perpendicular to the potential profile. Any control pulse of finite bandwidth will certainly create excitations away from zone center.

Loss of wave packet coherence represents a significant obstacle towards exercising quantum control in semiconductor heterostructures. Any scattering (manifested as phase-breaking collisions) results in loss of wave-packet coherence and places an upper limit upon our ability to manipulate coherent charge motion in these systems. In a typical experiment, loss of wave-packet coherence results in a reduction of

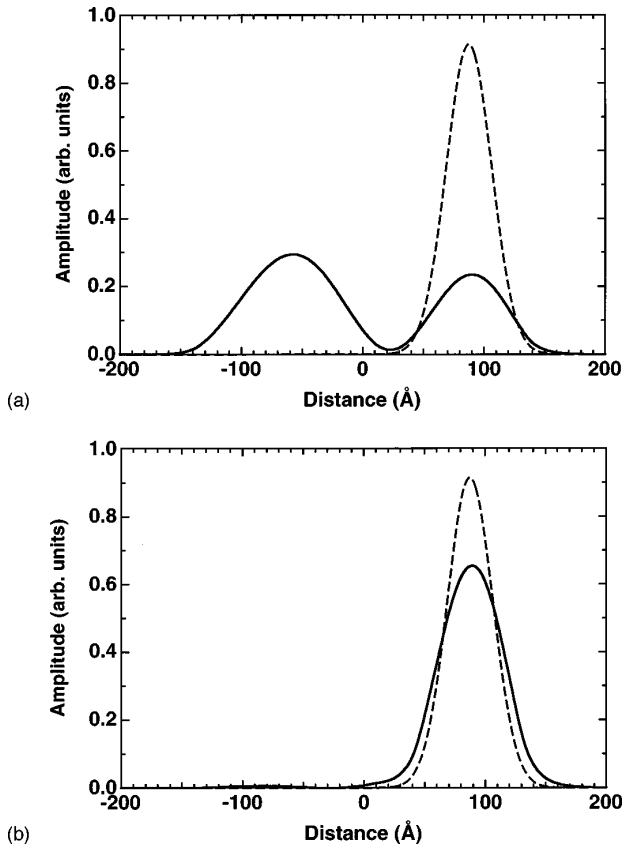

FIG. 8. Wave packet (solid line) at the target time vs target (dashed line). Panel (a) shows the results for a laser pulse chosen arbitrarily, such that the achievement is relatively low. Panel (b) shows the results when the parameters of the quantum well are allowed to vary, for the same pulse as in panel (a). The achievement is dramatically improved.

the coherent signal (THz emission, four wave mixing, electro-optic detection, etc.) over time. Transverse relaxation times are governed by specific scattering mechanisms. Free carrier dephasing can occur on time scales of 100 fs or less due to elastic intravalley and intervalley carrier-carrier scattering. Inelastic scattering of carriers with LO phonons, and carrier-defect scattering occur on somewhat longer time scales (100–500 fs). Controlling coherent free carrier motion will probably be difficult, since the oscillation period of the wave packet ($\sim$550 fs) in the ADQW is many times the carrier-carrier scattering time. Previous experiments have circumvented this difficulty by creating excitonic wave packets.[6,9] Excitonic dephasing times (due to exciton-exciton and exciton-phonon scattering) in quantum wells are typically a few picoseconds at low carrier densities ($n_e \sim 10^9$ cm^{-2}) and temperatures ($T<10$ K). Defect and impurity scattering also play important roles, since the homogeneity of the quantum well sample can influence dephasing times sensitively.

To first order, each scattering mechanism can be approximated by an exponential decay of the coherent signal, with relevant scattering mechanisms represented by phenomenological time constants. This approach has been used previously, for example, in solving the semiconductor Bloch equations for wave-packet dynamics in single quantum wells.[28] One of the key issues to be addressed in future work

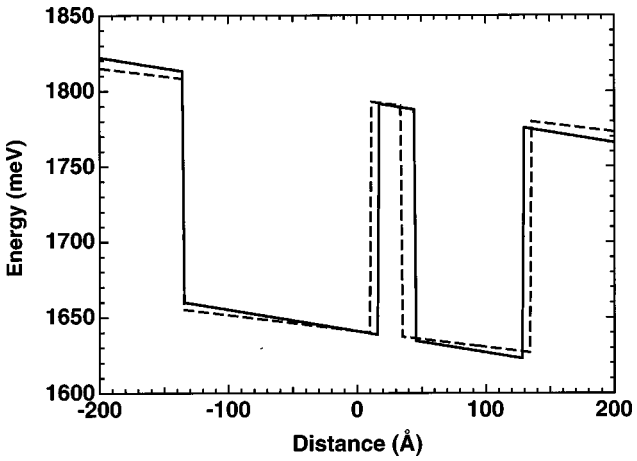

FIG. 9. Original quantum well potential (dashed line) vs optimized potential (solid line). The original potential, for a fixed laser pulse, produced the wave packet in Fig. 8(a) at the target time, while the optimized potential, for the same laser pulse, produced the final wave packet in Fig. 8(b).

is to what extent dephasing can be overcome by a suitably chosen control field. It may also be possible, or in some cases desirable, to exert control in cases in which the physical system is incoherent. Then, for some applications and target states, it may not be necessary to minimize dephasing effects. For example, control of charge transport in devices (incoherent charge motion) can be contemplated using THz radiation as a time-varying bias source in double or multiple well structures to tune the electronic levels into or out of tunneling resonance.

The most serious approximation in the numerical examples presented in this work is the assumption that the excitation is from a single heavy hole state at zone center (i.e., $k=0$). In reality, confinement of the hole states in the potential well lifts the heavy and light hole degeneracy at zone center and splits the energy levels. For the biased ADQW considered here, the confinement results in a splitting of about 5 meV, which is smaller than the splitting of the conduction-band levels. Therefore, excitation by a broadband pulse creates both heavy-hole and light-hole excitons that can undergo quantum beating and interference,[6] and thus modify the wave-packet dynamics. In addition, if the bandwidth of the laser pulse is large enough, a superposition of hole states can be created in the valence band, which will also form a time-dependent wave packet. The presence of both types of oscillating wave packets has been shown to contribute to coherent THz emission from ADQWs.[7]

We must also consider how nonzero k states affect the coherent dynamics. A optical pulse with finite bandwidth creates a distribution of excitations away from zone center with slightly different energies. The observed dynamic signal should then be computed as an integration over k. Since these excitations are created coherently and have small energy differences with respect to the mean energy of the distribution, we do not expect the dynamics to be altered appreciably, except while the field is on.

V. CONCLUSIONS

We have shown in this paper that electronic wave packets and THz radiation in quantum wells can be controlled with

simple, experimentally feasible laser pulses. The parameters of the pulses are optimized with a genetic algorithm that rapidly discovers the optimal field for a chosen target. The targets considered here are simple, but the method is quite general, and could be used, for example, to produce shaped THz pulses with complicated wave forms, from suitably complex potentials. Such pulses have potential applications in spectroscopy and communication.

As a starting point for exploring coherent control in heterostructures, the dc-biased ADQW structure considered here has the advantage of dynamical and computational simplicity. As we have shown, appropriate laser pulses can enhance (or suppress) the magnitude of the coherent oscillations of the coupled conduction-band well levels and the resulting THz emission. However, the dynamical ''phase space'' of the ADQW is quite limited since only two states participate in the creation of the coherent superposition state. This constraint forces the wave packet to exhibit simple oscillatory behavior and defeats any attempts to coerce the wave packet to display more complicated dynamics.

From a control standpoint, quantum systems composed of multiple states offer much greater flexibility and than the two-state ADQW. The dynamical behavior of the system becomes correspondingly more complex as the number of eigenstates available for coherent coupling increases. Future work will consider control in superlattices, dc-biased chirped superlattices (an extension of the biased ADQW), and single, asymmetric quantum wells. These systems are ideal candidates for implementing quantum control, precisely because their complexity does not allow for simple, intuition-guided experiments.

The calculations discussed in this work make definite predictions for experiments, which can be tested immediately in the laboratory. Success in these simple, proof-of-principle experiments will provide a framework for a number of additional studies. For example, samples with multiple wells (superlattices) will allow studies of tunneling and exciton dynamics in extended systems, where dephasing and Coulomb interactions are expected to have significant effects. Control of Bloch oscillations is also an intriguing possibility. To overcome uncertainties in both the theory and the experiments, the experiments will employ a feedback loop based on a learning algorithm.[38] This should enable a detailed analysis of which aspects of the physics most sensitively affect the dynamics, and will undoubtedly lead to new opportunities to better understand, and ultimately control, ultrafast semiconductor dynamics.

ACKNOWLEDGMENTS

Acknowledgment is made to the Donors of The Petroleum Research Fund, administered by the American Chemical Society, for partial support of this research. D.H.R. gratefully acknowledges the support of the National Science Foundation (ECS-9409297) and the Research Corporation. This work was partially supported by the U.S. Office of Naval Research through Grant No. N0091-J-1956, and by the National Science Foundation through Grant No. DMR-9520191. C.J.S. gratefully acknowledges support from the Alfred P. Sloan Foundation.

[1] P. Leisching, P. H. Bolivar, W. Beck, Y. Dhaibi, F. Brüggermann, R. Schwedler, H. Kurz, K. Leo, and K. Köhler, Phys. Rev. B **50**, 14 389 (1994).

[2] T. Dekorsy, R. Ott, H. Kurz, and K. Köhler, Phys. Rev. B **51**, 17 275 (1995).

[3] K. Leo, T. C. Damen, J. Shah, E. O. Göbel, and K. Köhler, Appl. Phys. Lett. **57**, 19 (1990).

[4] S. T. Cundiff, A. Knorr, J. Feldmann, S. W. Koch, E. O. Göbel, and H. Nickel, Phys. Rev. Lett. **73**, 1178 (1994).

[5] J. Feldmann, M. Koch, E. O. Göbel, F. Jahnke, T. Meier, W. Schäfer, P. Thomas, S. W. Koch, H. Nickel, S. Luttgen, and W. Stolz, Semicond. Sci. Technol. **9**, 1965 (1994).

[6] K. Leo, J. Shah, E. O. Göbel, T. C. Damen, S. Schmitt-Rink, W. Schäfer, and K. Köhler, Phys. Rev. Lett. **66**, 201 (1991).

[7] H. G. Roskos, M. C. Nuss, J. Shah, K. Leo, D. A. B. Miller, A. M. Fox, S. Schmitt-Rink, and K. Köhler, Phys. Rev. Lett. **68**, 2216 (1992).

[8] A. Bonvalet, J. Nagle, V. Berger, A. Migus, J.-L. Martin, and M. Joffe, Phys. Rev. Lett. **76**, 4392 (1996).

[9] P. C. M. Planken, I. Brener, M. C. Nuss, M. S. C. Luo, and S. L. Chuang, Phys. Rev. B **48**, 4903 (1993).

[10] M. S. C. Luo, S. L. Chuang, P. C. M. Planken, I. Brener, and M. C. Nuss, Phys. Rev. B **48**, 11 043 (1993).

[11] E. Dupont, P. B. Corkum, H. C. Liu, M. Buchanan, and Z. R. Wasilewski, Phys. Rev. Lett. **74**, 3596 (1995).

[12] R. Atanasov, A. Hache, J. L. P. Hughes, H. M. van Driel, and J. Sipe, Phys. Rev. Lett. **76**, 1703 (1996).

[13] A. P. Heberle, J. J. Baumberg, and K. Köhler, Phys. Rev. Lett. **75**, 2598 (1995).

[14] A. M. Weiner, J. Opt. Soc. Am. B **11**, 2480 (1994).

[15] I. Brener, P. C. M. Planken, M. C. Nuss, M. S. C. Luo, S. L. Chuang, L. Pfeiffer, D. E. Leaird, and A. M. Weiner, J. Opt. Soc. Am. B **11**, 2457 (1994).

[16] S. I. Yakovlenko, Zh. Eksp. Teor. Fiz. **64**, 2020 (1973) [Sov. Phys. JETP **37**, 1019 (1973)].

[17] W. S. Warren, H. Rabitz, and M. Dahleh, Science **259**, 1581 (1993).

[18] D. J. Tannor and S. A. Rice, Adv. Chem. Phys. **70**, 441 (1988).

[19] M. Shapiro and P. Brumer, Int. Rev. Phys. Chem. **13**, 187 (1994).

[20] D. Neuhauser and H. Rabitz, Acc. Chem. Res. **26**, 496 (1993).

[21] J. L. Krause, R. M. Whitnell, K. R. Wilson, and Y. J. Yan, in *Femtosecond Chemistry*, edited by J. Manz and L. Wöste (VCH, Weinheim, 1995), pp. 743–779.

[22] A. M. Weiner, J. P. Heritage, and E. M. Kirschner, J. Opt. Soc. Am. B **5**, 1563 (1988).

[23] C. W. Hillegas, J. X. Tull, D. Goswami, D. Strickland, and W. Warren, Opt. Lett. **19**, 737 (1994).

[24] M. M. Wefers and K. A. Nelson, Opt. Lett. **18**, 2032 (1993).

[25] A. E. Efimov, C. Schaffer, and D. H. Reitze, J. Opt. Soc. Am. B **12**, 1968 (1995).

[26] A. M. Weiner, D. E. Leaird, G. P. Wiederrecht, and K. A. Nelson, Science **247**, 1317 (1990).

[27] P. C. M. Planken, M. C. Nuss, I. Brener, K. W. Goossen, M. S. C. Luo, S. L. Chuang, and L. Pfeiffer, Phys. Rev. Lett. **69**, 3800 (1992).
[28] A. V. Kuznetsov, G. D. Sanders, and C. J. Stanton, Phys. Rev. B **52**, 12 045 (1995).
[29] J. L. Krause, M. Messina, K. R. Wilson, and Y. J. Yan, J. Phys. Chem. **99**, 13 736 (1995).
[30] H. Rabitz and S. Shi, Adv. Molec. Vib. Coll. Dyn. **1A**, 187 (1991).
[31] S. Shi and H. Rabitz, Chem. Phys. **139**, 185 (1989).
[32] S. H. Tersigni, P. Gaspard, and S. A. Rice, J. Chem. Phys. **93**, 1670 (1990).
[33] R. Kosloff, S. A. Rice, P. Gaspard, S. Tersigni, and D. J. Tannor, Chem. Phys. **139**, 201 (1989).
[34] M. Shapiro and P. Brumer, Chem. Phys. Lett. **208**, 193 (1993).
[35] J. Somlói, V. A. Kazakov, and D. J. Tannor, Chem. Phys. **172**, 85 (1993).
[36] Y. J. Yan, R. E. Gillilan, R. M. Whitnell, K. R. Wilson, and S. Mukamel, J. Phys. Chem. **97**, 2320 (1993).
[37] J. L. Krause, R. M. Whitnell, K. R. Wilson, Y. J. Yan, and S. Mukamel, J. Chem. Phys. **99**, 6562 (1993).
[38] R. S. Judson and H. Rabitz, Phys. Rev. Lett. **68**, 1500 (1992).
[39] J. D. Grefenstette, GENESIS v5.0, Copyright (c), 1990.